Advanced Composites and Hybrid Materials (2022) 5:2787–2800
https://doi.org/10.1007/s42114-022-00564-6

RESEARCH

Improvement of thermodynamic properties of poly(butanediol sebacate-butanediol terephthalate) (PBSeT) composites based on the dispersion of $PCaCO_3$@tannic acid formed by complexation of tannic acid and Ti

Tong Liu[1] · Zhimao Li[1,2] · Tianxiang Jiang[3] · Shaohua Xi[4] · Yingchun Li[1] · Jiang Guo[4] · Mina Huang[5,6] · Hassan Algadi[7] · Xinming Ye[1] · Qinglong Jiang[6]

Received: 10 August 2022 / Revised: 18 September 2022 / Accepted: 23 September 2022 / Published online: 13 October 2022

Abstract

Poly(butanediol sebacate—butanediol terephthalate) (PBSeT) has the excellent biodegradability. And nano-CaCO3 modified by titanate coupling agent is frequently added into polymers as an additive to reduce costs. In this research, the PBSeT-based composite was prepared by the melt blending method. Compared with PBSeT, the maximum thermal decomposition temperature, Young's modulus, and glass transition temperature of the composite material were advanced by 12.67 ℃, 64.5%, and 10.36 ℃ when the content of tannic acid (TA) was 2, 4, and 6 wt%, respectively. Peculiarly, the puncture load of the composite was increased by 71.7% when the TA was 8 wt%; meanwhile, the degradation performance and water absorption performance were also better than other composites. Based on the comprehensive analysis of the experimental results, a complex named $PCaCO_3$@TA was formed by interacting TA with Ti from the titanate coupling agent and coated the surface of nano-$CaCO_3$ to change the dispersion of nano-CaCO3. Moreover, glycerol is mainly concentrated in the BSe segment as polyphenol membrane attracting the secondary hydroxyl group from the unreacted glycerol.

Keywords Nano-$CaCO_3$ · Tannic acid · Thermal stability · Puncture load · Biodegradable materials

1 Introduction

Due to the low prices and excellent physical as well as chemical properties, the wide applications of plastics in various industries are keep increasing [1–4]. Nonetheless, the consumption of petroleum resources is exacerbating, which is the main monomer source for plastics. Furthermore, plastic-related issues are rapidly increasing since most of the plastics are non-biodegradable [5–9], such as plastic waste disposal and incineration caused harmful gases and smoke, and the interference various biological hormones in the environment. Therefore, it is urgent to develop environment

✉ Yingchun Li
liyingchun@nuc.edu.cn

✉ Jiang Guo
jguo@sust.edu.cn

✉ Qinglong Jiang
jiangq@uapb.edu

[1] School of Materials Science and Engineering, North University of China, Taiyuan 030051, China

[2] Beijing Engineering Research Centre of Cellulose and Its Derivatives, Beijing 100081, China

[3] School of Materials Science and Engineering, Nanjing University of Posts and Telecommunications, Nanjing 210003, China

[4] School of Materials Science and Engineering, Shaanxi Key Laboratory of Green Preparation and Functionalization for Inorganic Materials, Shaanxi University of Science & Technology, Xi'an 710021, China

[5] College of Materials Science and Engineering, Taiyuan University of Science and Technology, Taiyuan 030024, China

[6] Department of Chemistry and Physics, University of Arkansas, Pine Bluff, AR 71601, USA

[7] Department of Electrical Engineering, College of Engineering, Najran University, Najran 11001, Saudi Arabia

friendly and biodegradable plastic materials to address the mentioned problems [10]. Among them, two solutions were proposed by the scientists: the first is to avoid the consumption of non-renewable resources by using polymer monomers obtained from nature; and the second is to design polymers with a biodegradable backbone. Based on these strategies, traditional plastics have recently been gradually replaced by some biodegradable plastics, such as poly(lactic acid) (PLA) [11], poly(butylene succinate) (PBS) [12], poly(butylene adipate-co-terephthalate) (PBAT) [12–14], and poly(butylene sebacate-co-terephthalate) (PBSeT) [15]. At present, the innovative manufacturing strategies and possibilities accelerated the use of different kinds of biological materials in 3D printing or additive manufacturing, in order to replace the modern/classic plastic filament to mitigate the issue of sustainability [16, 17].

PBSeT is synthesized from sebacic acid, terephthalic acid, and 1,4-butanediol by esterification and condensation polymerization. PBSeT is used as an upgraded product of PBAT due to the large amount of biomass source for sebacic acid. However, PBSeT has worse thermodynamic properties comparing with PBAT, such as tensile strength, Young's modulus, puncture load, tear strength, and glass transition temperature, which is from the longer carbon chain of sebacic acid than that of adipic acid. Scientists have proposed many solutions: the content of terephthalic acid was increased during synthesis; however, it cannot be degraded when the content exceeds 50% [18]; PBSeT is blended or grafted with PLA; however, the compatibility is relatively poor, and the mechanical properties are reduced [19, 20]; the thermodynamic properties of the composite material are not substantially changed by the low content of PBT added to PBSeT [21]. In addition, for another important reason, the development of PBSeT will be restricted due to the high price of sebacic acid.

The cheap $CaCO_3$ is commonly used as a reinforcing material combined with different polymers to produce composite materials [22, 23]. However, nano-$CaCO_3$ is often modified to obtain better dispersibility due to its poor dispersibility [5, 24]. Still, modified nano-$CaCO_3$ agglomerates when the content exceeded 10%. Furthermore, the large amount of nano-$CaCO_3$ brings in many properties declined, such as tensile strength, puncture strength, degradation properties and so on. Therefore, the dispersion of high-content nano-$CaCO_3$ has become one of the difficult problems for scientists and manufacturers. Tannic acid is an additive obtained from gallnut, which possesses the structure of polyhydroxyl and polybenzene rings, and widely used in medicine, food, flame-retardant industries [25–27]. The special structure formed by Ti ions of nano-CaCO3 modified by tannic acid and titanate coupling agents was utilized to enhance the interaction with the polyester material, thus improving the dispersibility.

In our recent studies, PBSeT with minimal content of different cross-linking agents via two-step esterification and polycondensation was synthesized [28]. We found that the mechanical properties and crystallinity of materials were improved by glycerol in these kinds of cross-linking agents [29]. In addition, PBSeT added with glycerol could be degraded within a certain range of 0 to 60 mol %, even if the content of the added terephthalic acid exceeded 50 mol %, which greatly facilitated the degradation performance of PBSeT with high terephthalic acid content and its significance for the promotion of PBSeT [30]. Unfortunately, there is no valid evidence indicating where the glycerol binds in polyester materials and how it affects material properties.

In this paper, PBSeT with glycerol as cross-linking agent was used as the matrix material and mixed with nano-$CaCO_3$ and tannic acid to a new composite material by melt blending. To improve the dispersibility of nano-$CaCO_3$, a complex is formed from the Ti ions of nano-$CaCO_3$ with tannic acid, which increases the interaction force between the matrix material and nano-$CaCO_3$ while reducing the cost. Moreover, it is proved that the binding sites of glycerol are mainly concentrated in the BSe segment of the PBSeT material.

2 Experimental

2.1 Materials

Sebacic acid (SeA), nano-$CaCO_3$, tannic acid (TA), glycerol (GL), tetrabutyl titanate, and lipase were from Hengshui Jinghua Chemical Industry Co., Guangxi Kelong Powder Co., Shanghai Macklin Biochemical Co., Tianjin Guangfu Technology Development Co., Wuxi Yatai United Chemical Co., and Houzhuang Industrial Park, Xinzheng City, Zhengzhou City, Henan Province, respectively. Furthermore, terephthalic acid (TPA) and 1,4-butanediol (BDO) were used as received.

2.2 Synthesis of PBSeT copolyester

PBSeT copolyester, with glycerol (GL) unit used as crosslinking reagents (0.06 mol), was synthesized from BDO and dicarboxylic acid (7 mol, SeA: TPA = 5:5) via two-step esterification followed by melt polycondensation. In brief, as shown in Scheme 1A, the four monomers (among BDO for 5 mol) were added into a 5-L reaction kettle under mechanical stirring and normal pressure and then heated to 170 ~ 190

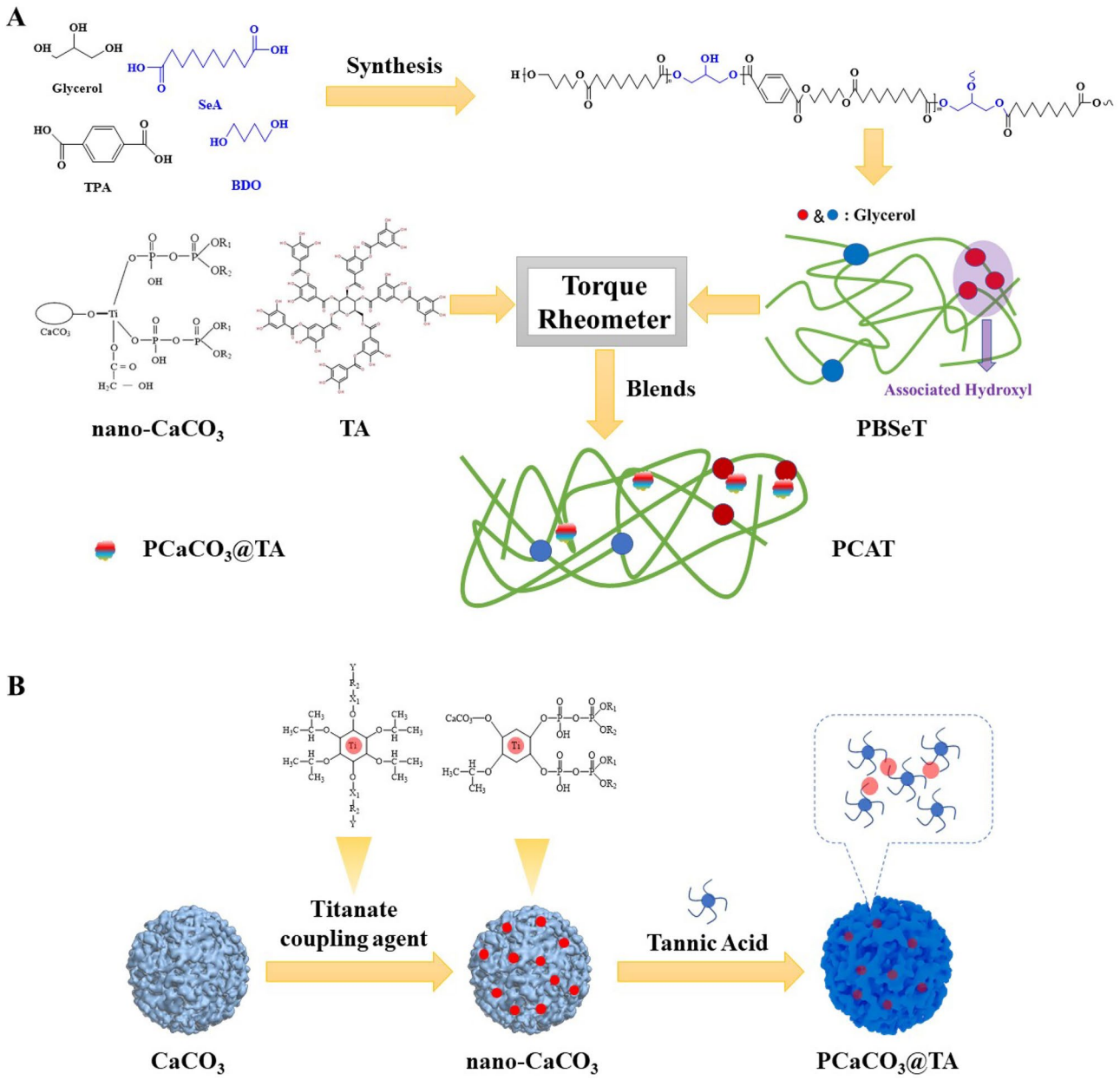

Scheme 1 **A** Synthesis of PBSeT and preparation of PBSeT-based composite materials (PCAT); **B** $PCaCO_3$@TA was formed by tannic acid complexed with Ti

℃ as the first esterification temperature lasting for 1.5 ~ 2 h. TBOT (0.3% mol of dicarboxylic acid) and BDO (5 mol) were added with raising the temperature to 210 ~ 230 ℃, and the second esterification reaction was conducted for 3 ~ 4 h until the produced water was close to the theoretical water. Finally, the polycondensation reaction was performed under vacuum (220 ~ 700 Pa) at 230 ~ 245 ℃ for 5–6 h until Weissenberg effect emerged. The products were vacuum-dried at 60 ℃ for more than 24 h and stored in a desiccator before testing.

2.3 Preparation of PBSeT-based composite materials (PCAT)

PBSeT pellets were dried at 60 ℃ for 12 h under vacuum prior to use and then mixed with 20 wt% of nano-$CaCO_3$ and 0, 2, 4, 6, 8, and 10 wt% of TA by the torque rheometer (RTOI-20/10, Guangzhou Putong Experimental Analytical Instrument Co.) at 170 ~ 200 ℃, as shown in Scheme 1A. These composites PBSeT, nano-$CaCO_3$, and TA were denoted as PCAT-0, PCAT-2, PCAT-4, PCAT-6, PCAT-8,

and PCAT-10, respectively, as shown in Table 1. In addition, it was worth noting that the melt blending lasted for 3 ~ 5 min.

2.4 Characterizations

2.4.1 Fourier transform infrared spectroscopy (FTIR)

The FTIR spectra of PCAT composites were recorded on a Nicolet iS10 spectrometer (Thermo Fisher Scientific, USA). The spectra were recorded from 4000 to 600 cm^{-1} at a resolution of 4 cm^{-1} over 32 scans.

2.4.2 X-ray diffraction analysis (XRD)

X-ray diffraction (XRD) pattern was recorded using a RIGAKU X-ray diffraction system (D/max-Rb) with Cu radiation (1.54 Å), working at 40 kV and 100 mA. All samples were scanned from 10 to 70° (2θ) with a step size of 0.02°and an acquisition time of 30 s per step.

2.4.3 Differential scanning measurement thermal analysis (DSC)

Thermal transition behaviors were recorded with differential scanning calorimetry (DSC-1, METTLER TOLEDO) under a nitrogen. Approximately 6–8 mg of the sample was tested under a standard heat-cool-heat cycle from − 50 to 190 ℃; both heating and cooling rates were 10 ℃/min. The temperature was held at 190 ℃ for 5 min before cooling.

2.4.4 Thermogravimetric analysis (TGA)

Thermogravimetric analysis (TGA) measurements were carried out under a nitrogen atmosphere by a thermal analyzer (TGA-2, METTLER TOLEDO) from 10 to 900 ℃ at a 10 ℃/min heating rate.

2.4.5 Mechanical performance test

Tensile properties were measured with a CMT6104 universal testing machine at a tensile speed of 50 mm/min. Dumbbell-shaped tensile specimens were prepared by injection molding. All the specimens were kept in a standard atmosphere of 25 ℃ for at least 24 h before testing. At least five specimens ($25 \times 4.8 \times 1.9$ mm^3) were tested for each sample, and all the reported properties were presented average values of all the trials.

The puncture performance was measured with a CMT6104 universal testing machine using a steel needle with a diameter of 1.0 mm and a radius of 0.5-mm spherical tip at a puncture speed of 50 mm/min. Round puncture specimens (diameter = 35 cm, thickness = 0.55 mm) were prepared by thermal compression.

As specified in ISO 34–1:2004(GB/T 529–2008, China), all composites were tested for tearing strength using a CMT6104 universal testing machine (Shenzhen New Sansi Material Testing Co., Ltd.). The test was conducted using a constant tearing rate of 100 ± 10 mm/min. The notch with depth of 40 ± 5 mm is located in the center of the specimen width. These samples had a size of 100 mm × (15 ± 1) mm.

Table 1 Composite material formula

Sample	Tannic acid (wt%)	PBSeT (wt%)	nano-$CaCO_3$ (wt%)
PBSeT	0	100	0
PCAT-0	0	80	20
PCAT-2	2	78	20
PCAT-4	4	76	20
PCAT-6	6	74	20
PCAT-8	8	72	20
PCAT-10	10	70	20

2.4.6 Rheological measurements

The rheological properties were measured via DHR-2 mold rotary rheometer (Waters, USA) with the parallel plate geometry of 25 mm in diameter. The frequency sweep range was from 0.01 to 100 Hz under a strain of 1.0%. Meanwhile, the test temperature was 130 ℃.

2.4.7 Water absorption test

The water absorption test of these composite materials was tested on the basis of GB/T 1043–2008. Samples were cut into 10 mm × 10 mm pieces and dried in a blast drying oven at 60 ℃ for 48 h. Firstly, original mass of sample was recorded as m_1. In quick succession, the sample was completely immersed in distilled water at room temperature and wiped off with filter paper after 24 h, whose quantity was recorded as m_2. Water absorption rate (WAR) was calculated with formula as follows:

$$WAR = \frac{m_2 - m_1}{m_2} \times 100\%$$

2.4.8 Enzyme degradation test

The enzymatic degradation was tested by lipase from the market. All samples in the form of slices $100 \times 100 \times 0.55$ mm were prepared by first hot-pressing and then cold-pressing under a square mold (the average thickness was 0.55 mm) and cut into $20 \times 20 \times 0.55$ mm size. Whereafter, they were placed in Schott bottle containing phosphate buffer solution (pH = 7.2) with 0.8 mg/mL lipase at room temperature. After

a specific period of incubation, the slices were removed and washed with distilled water and weighted with electronic balance (FA2004N, Shanghai Qinghai Instrument Co.) until a constant weight was reached. The degree of biodegradation was estimated from the weight loss.

2.4.9 Scanning electron microscope analysis (SEM)

The morphology of these composites was examined by a field emission scanning electron microscope (JEOL JSM-7200F, Japan). The C, O, Ca, and Ti element mapping was verified by energy-dispersive X-ray spectroscopy (EDXS Oxford x-max). All samples before and after enzymatic degradation surface of samples were gold-coated before test.

2.4.10 Water contact angle test

For contact angle testing, these composite samples were fixed on glass slides using double-sided tape, ensuring that the surface of samples was flat. Using a 1-mL syringe, a standard drop of 4 μL was used to apply de-ionized water droplets to each copolyester sample. The contact angle of the drops with respect to the flat surface was then measured each second for 9 s (allowing 1 s to equilibrate, total test 10 s) using Attention Theta Lite Automatic microscopic contact angle measuring instrument.

Data were obtained from the average values of the five samples measured. Data analysis used a single correlation analysis method, where the error was the standard deviation.

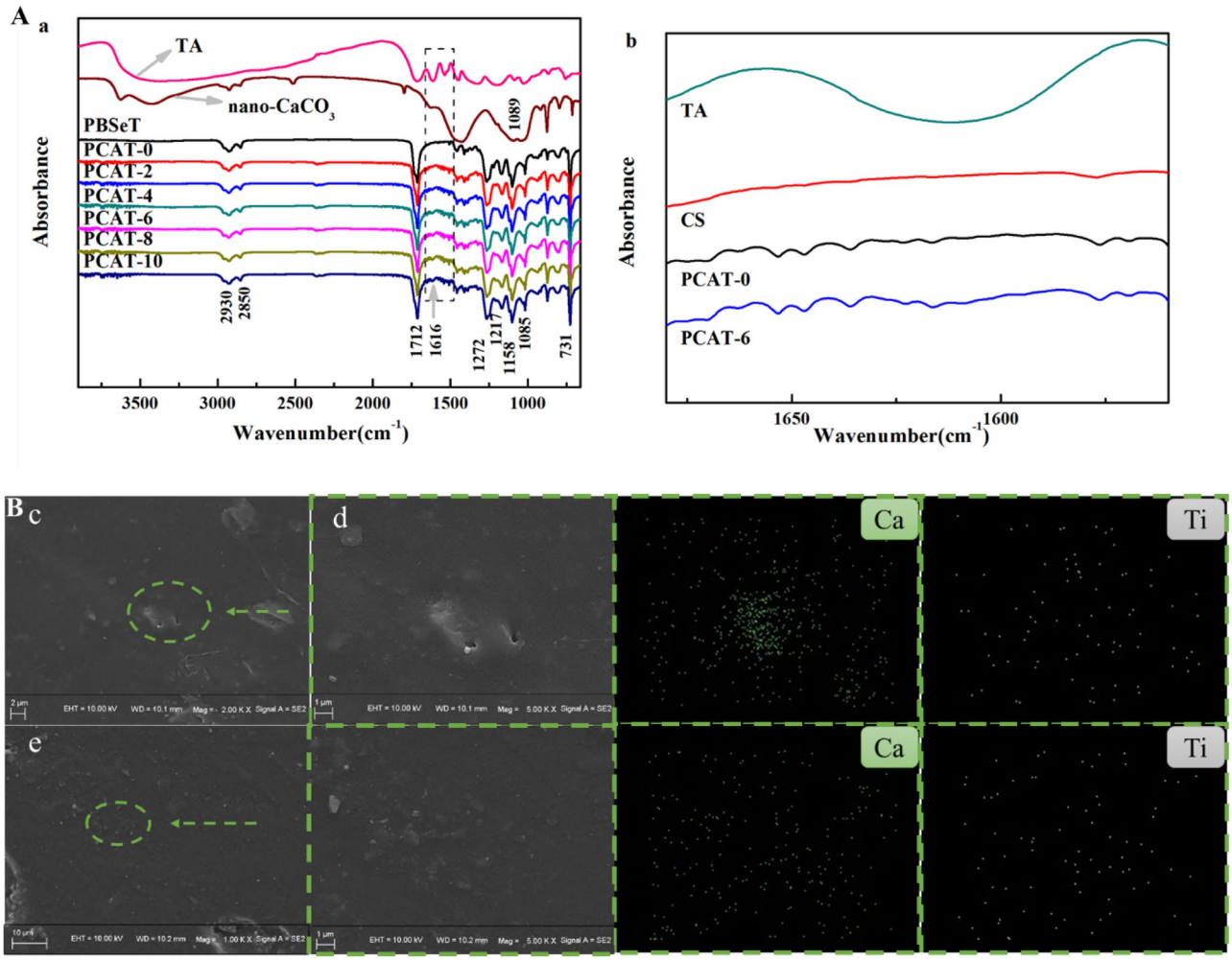

Fig. 1 **A** FTIR spectra of composites with different proportions of tannic acid addition (**a** and **b**); **B** SEM images and the corresponding elemental map of PCAT - (0: **c**, **d**; 8: **e**, **f**)

3 Results and discussion

3.1 Surface chemical composition analysis

FTIR spectroscopy was used to characterize the surface chemical composition of these composites and the influence of TA on these materials. As can be seen from Fig. 1A, there was no obvious infrared absorption peak in the 3300 ~ 3500 cm^{-1} from the composites, indicating that nano-$CaCO_3$ particles were not apparently exposed on the surface of composites and were enshrouded by PBSeT molecular. As illustrated in SEM images (Fig. 1d and f), the dispersibility of calcium carbonate improved and was not exposed to the surface of the material, when TA was added to composites. Similarly, this peak was not distinctly showed by composite of PLA/PBAT after adding MCC, which was reported by Zhang et al. [31]. Clearly, typical absorption bands of aliphatic (2930 and 2850 cm^{-1}) are shown. In addition, the contractile vibration of C = O at 1712 cm^{-1}, stretching vibration of C–O–C at 1085 and 1217 cm^{-1}, the peak of aromatic C-O (1272 and 1158 cm^{-1}), and the stretching vibration absorption peak of C-H close to the benzene ring at 731 cm^{-1} are displayed. Furthermore, a more obvious benzene ring absorption peak at 1616 cm^{-1} was showed by these composites due to the added TA. This indicated that nano-$CaCO_3$ is encapsulated by TA, which was caused by a complex between TA and Ti ions (Scheme 1B). The related mechanism of complex formation was studied by Douxin Xiao et al. [32]. For the FTIR spectra of composite, Zhang et al. [33] also reported similar conclusions.

3.2 Thermal transition properties

These composites were examined by DSC to investigate their thermal transition properties. Typical DSC curves are shown in Fig. 2, and the thermal transition data are gathered in Table 2. Compared to PBSeT, it can be seen from Table 2 that the crystallinity of the PACT composites had been decreased, due to the hindrance of the movement of the chain segment by nano-$CaCO_3$. Nevertheless, the crystallinity of PCAT slightly went up with TA added, which was attributed to $PCaCO_3$@TA. In the cooling scan, the crystallization temperature of PCAT was increased and then slightly decreased on account of $PCaCO_3$@TA used as a nucleating agent to make PBSeT crystallize at a higher temperature; however, the crystallization temperature of PCAT was started to drop when the content of TA was exceeded 8%, as a result of the hydroxyl group of $PCaCO_3$@TA aggregated.

The heat resistance of these composites was influenced by the addition of $PCaCO_3$@TA. In the second heating, the glass transition temperature was increased and then decreased as the content of TA increased; the glass transition temperature was elevated by about 10 degrees, and the melting point of the lower temperature disappears when the content of TA was 6%. In the composites with added TA, the interaction between $PCaCO_3$@TA and the ester group of PBSeT leaded to the movement more difficult with the PBSeT chain segments. In the composites with exceeding 6% TA, the lower melting point corresponding to the BSe segment was disappeared, indicating that the interaction on $PCaCO_3$@TA with the ester group and the hydroxyl group

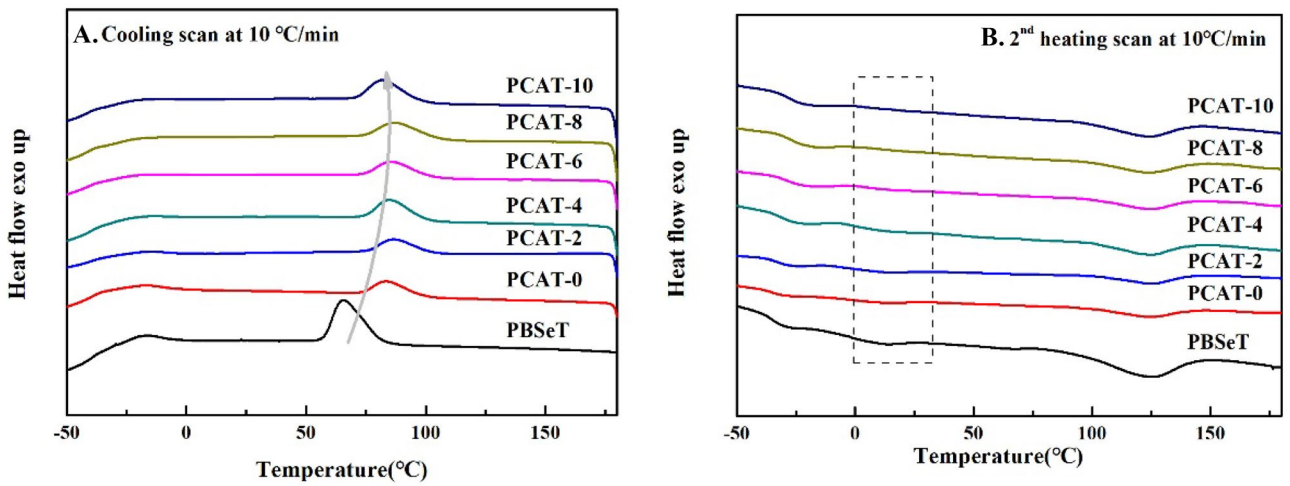

Fig. 2 DSC curves of composites with different proportions of tannic acid addition: **A** Cooling scan at − 10 °C/min, **B** 2nd heating scan at 10 °C/min

Table 2 DSC data of PCAT composites

Sample	Cooling scan			Second heating scan		
	T_C	ΔH_C	X_C%	T_g	T_m	ΔH_m
PBSeT	65.63/ – 16.62	21.12/4.10	14.3	– 34.63	10.77/124.02	1.53/15.15
PCAT-0	83.92/ – 16.63	9.41/4.53	7.1	– 35.78	12.63/124.06	1.23/5.31
PCAT-2	84.76/ – 15.47	12.76/2.55	8.7	– 31.32	18.35/125.92	2.13/7.37
PCAT-4	85.77/ – 16.96	12.51/1.63	8.0	– 29.12	17.93/123.87	1.05/7.35
PCAT-6	86.74/ – 17.13	11.90/1.23	7.4	– 24.27	- /124.22	- /6.83
PCAT-8	87.44/ – 18.96	10.62/1.01	6.6	– 26.45	- /123.53	- /6.05
PCAT-10	82.11/ – 18.63	13.22/0.85	8.0	– 26.46	- /123.37	- /8.11

was mainly focused on the BSe segment. Astonishingly, a piece of evidence above shows that the secondary hydroxyl group on the unreacted glycerol was mainly concentrated with BSe segment. Among them, the relationship between glycerol content and PBSeT copolyester was mentioned in our previous work [28]. On the contrary, $PCaCO_3$@TA did not seem to change anything for the BT segment with a higher melting point.

3.3 Crystal structure

XRD (Fig. 3) was conducted to verify the change of crystallinity and crystallographic form for these samples. PBSeT showed five different diffraction peaks, with a combination of amorphous and crystalline structure. The crystal peaks were observed at 16.2° (011), 17.4° (010), 20.4° (111), 23.1° (100), and 24.8° (101), whose crystal form was basically the same as that of PBAT [34, 35]. Surprisingly, the crystallinity of the composite was decreased by added nano-$CaCO_3$; however, when TA was added to the composite system, the crystallinity slightly increased, which was consistent with the results tested by DSC. The crystal peaks of nano-$CaCO_3$ were mainly concentrated at 29.4° (104), 39.4° (113), and 47.8° (116), which was obviously different from the crystal face index of the PBSeT. Moreover, the crystallinity was also obviously descended because of the higher content of nano-$CaCO_3$ 20 wt% [22]. Moreover, there were 20.4° (111) and 23.1° (100) (consistent with PBT) remaining crystal planes related to PBSeT in the composites. It can be seen that the crystalline part destroyed by nano-$CaCO_3$ was from the BSe segment. In addition, the crystallinity of the composites was enhanced by $PCaCO_3$@TA that might also

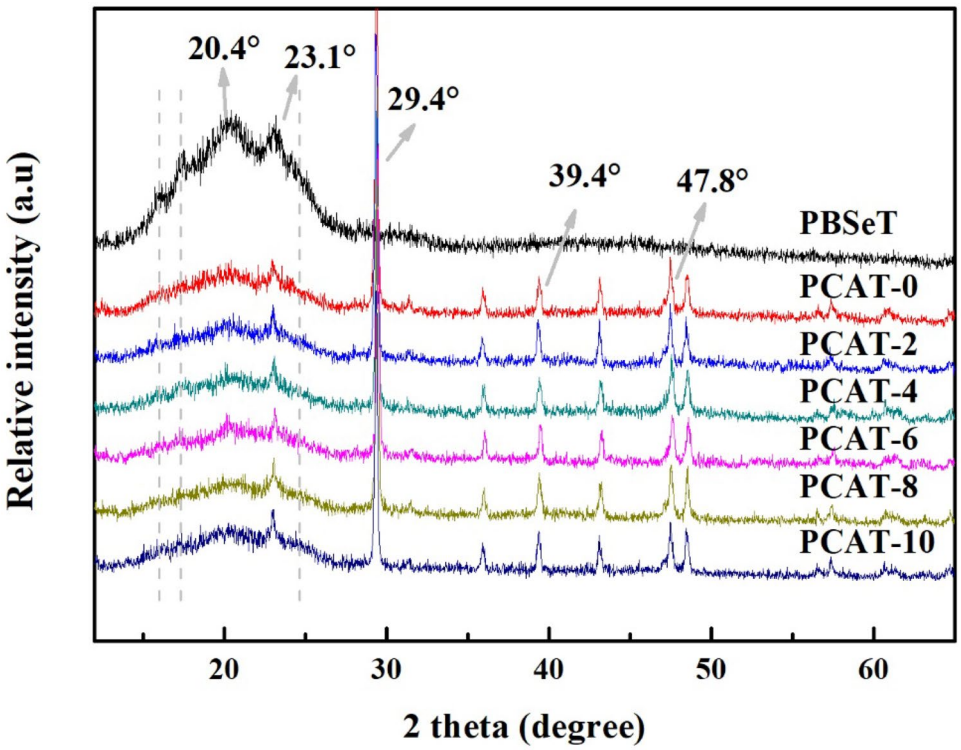

Fig. 3 XRD curves of composites with different proportions of tannic acid addition

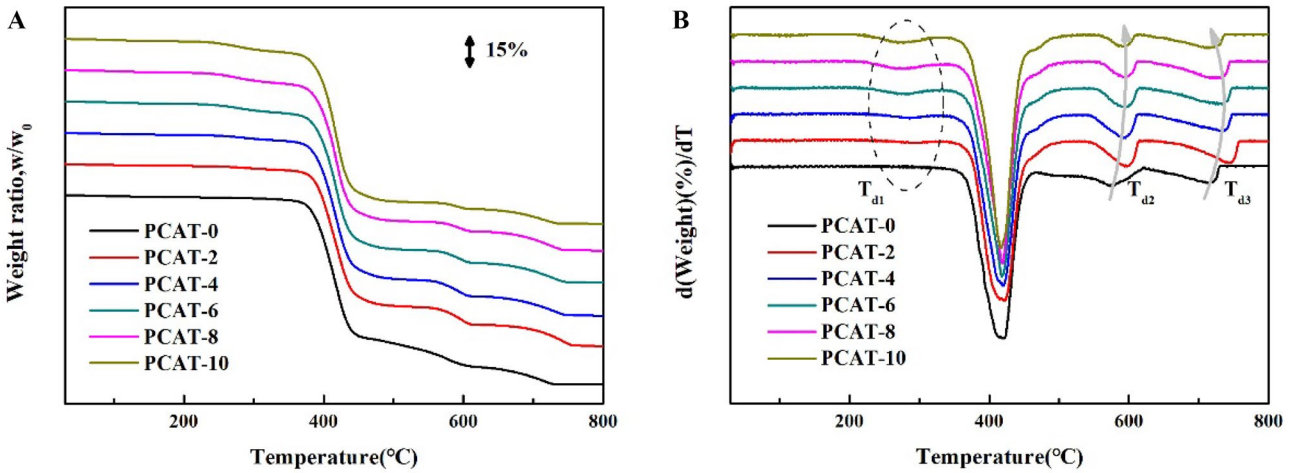

Fig. 4 **A** Thermogravimetric and **B** differential thermogravimetric curves of composites with different proportions of tannic acid addition (10 ℃/min, N_2)

appear at the BSe segment, as other three crystal planes connected with PBSeT were slightly shown, with the content of TA increased.

3.4 Thermal stability

The thermal stability of PCAT composites was evaluated by TGA under N_2 atmosphere, with PBSeT as a reference. The TGA curves are shown in Fig. 4. The decomposition temperature at 5% weight loss, maximum, primary, secondary, and tertiary decomposition rate ($T_{d,5}$, $T_{d,max}$, T_{d1}, T_{d2}, and T_{d3}) are listed in Table 3. Compared with PBSeT, the thermal decomposition of PACT was much more complicated. The analysis showed that T_{d1} was due to the addition of TA, and T_{d2} and T_{d3} were corresponding to added nano-$CaCO_3$. Particularly, PCAT-2 was showed different properties from other groups, which not only had the thermal stability improved by the addition of nano-$CaCO_3$, but also did not affect the decomposition temperature of $T_{d,5}$. It can be seen that the change of decomposition temperature caused by the gradual increase of TA was all caused by $PCaCO_3$@TA, which conclusively had an influence on PBSeT. In a word, there are interactions between them.

3.5 Mechanical properties

Mechanical property of materials plays key role in evaluating whether materials can meet the environment of use. The puncture load, extension at puncture, tearing strength, tensile strength, elongation at break, and Young's modulus of the composite material were tested, as shown in Figs. 5, 6, and Table 4, respectively.

From Fig. 5 and Table 4, the puncture load of the composite material was first improved and then decreased with the gradual addition of TA. When the content of TA arrived at 8 wt%, the puncture load reached to the maximum value, which was 1.72 times higher than that of PBSeT. Nevertheless, the tearing strength of the composite material was first decreased and then increased with the TA added. Thus, it could be seen that TA mainly played a role of cross-linking in nano-$CaCO_3$/PBSeT to enhance the puncture load of the material. Moreover, nano-$CaCO_3$ as an inorganic filler was beneficial to boost the Young's modulus of the material (Table 4), which would be the material that became difficult to be penetrated. In contrast, the tearing strength of the composite material was showed the opposite trend. Nano-$CaCO_3$ and PBSeT were always in a state of separation, and it is

Table 3 Characteristic decomposition temperatures of PCAT composites

Sample	$T_{d,5}$ (℃)	$T_{d,max}$ (℃)	T_{d1} (℃)	T_{d2} (℃)	T_{d3} (℃)	Residue at 900 ℃ (%)
PBSeT	375.02	408.00	-	-	-	3.16 (600 ℃)
PCAT-0	375.67	419.67	-	575.33	714.00	9.24
PCAT-2	376.30	420.67	-	596.33	743.00	12.50
PCAT-4	365.55	419.33	296.28	594.67	732.67	12.64
PCAT-6	320,09	419.00	290.34	593.67	731.00	12.99
PCAT-8	300.47	419.00	284.32	592.67	721.67	13.27
PCAT-10	300.20	417.33	278.35	591.67	713.00	10.46

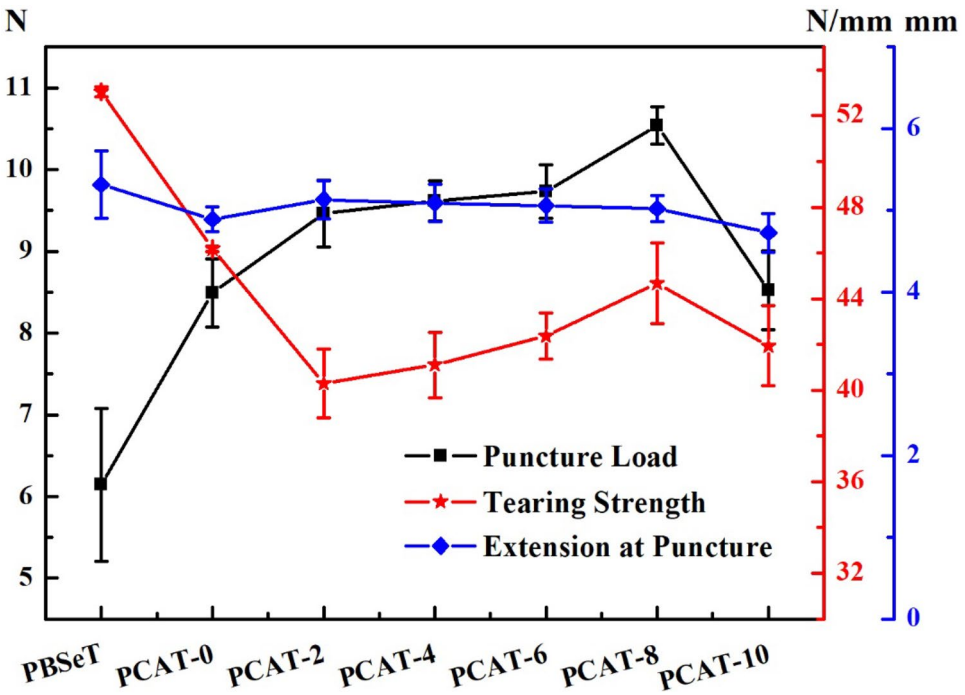

Fig. 5 Puncture load, extension at puncture, and tearing strength curves of composites with different proportions of tannic acid addition

fatal to the tearing strength of the composite. Oppositely, the interaction formed between $PCaCO_3$@TA and the matrix material was acted as a non-covalent bond cross-linking point to slightly raise the tearing strength of the material. However, the possibility of the tendency bettered was destroyed as a result of the agglomeration of nano-$CaCO_3$ as the content of TA reached 10 wt%. Fortunately, the extension at puncture remained the same.

Figure 6 and Table 4 showed the tensile strength, elongation at break, and Young's modulus of composite materials in terms of PBSeT, indicating the relationship between PCAT and the content of TA. The results showed that the tensile strength of PCAT decreased and then increased, as the ratio of TA increases. On the contrary, the Young's modulus was first raised and then decreased. The elongation at break of composite materials keeps declining. Thus, the

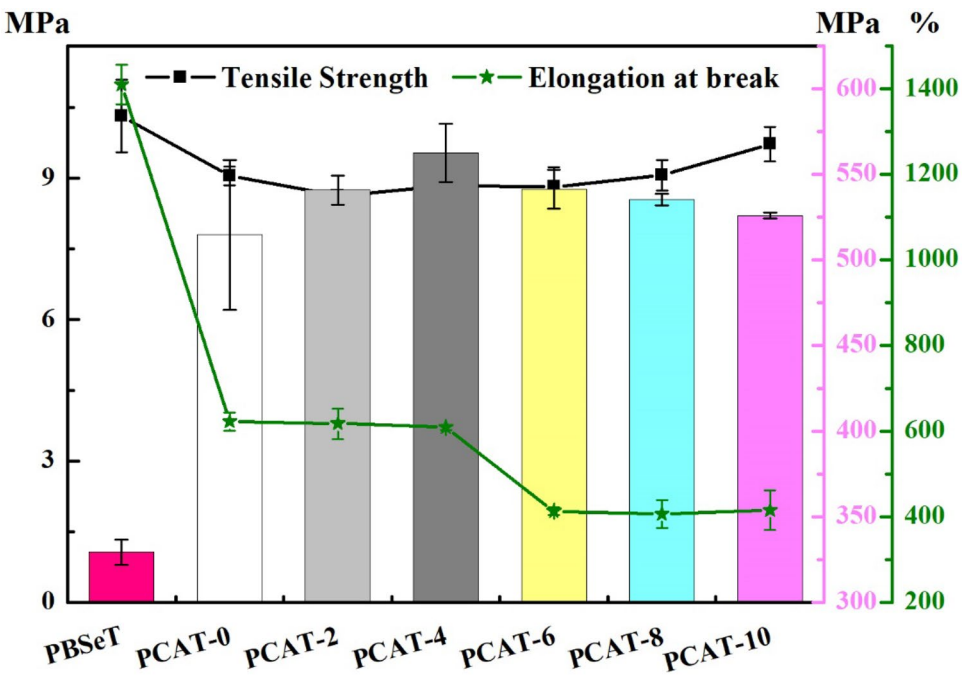

Fig. 6 Tensile strength, elongation at break, and Young's modulus curves of composites with different proportions of tannic acid addition

Table 4 Mechanical properties of PCAT composites

Sample	E(Mpa)	δ_b(Mpa)	ε_b(%)	T_S(N/mm)	F_p(N)	Ext(mm)
PBSeT	329.29 ± 7.33	10.32 ± 0.77	1343.81 ± 158.36	53.05 ± 0.21	6.14 ± 0.94	5.31 ± 0.41
PCAT-0	514.62 ± 43.66	9.05 ± 0.19	622.52 ± 21.58	46.18 ± 0.11	8.49 ± 0.42	4.89 ± 0.15
PCAT-2	540.84 ± 8.39	8.63 ± 0.09	618.07 ± 35.58	40.19 ± 1.5	9.46 ± 0.41	5.13 ± 0.24
PCAT-4	562.63 ± 17.06	8.84 ± 0.43	609.00 ± 6.41	41.11 ± 1.42	9.62 ± 0.24	5.09 ± 0.23
PCAT-6	541.52 ± 11.42	8.81 ± 0.42	413.08 ± 9.05	42.37 ± 1.01	9.73 ± 0.33	5.06 ± 0.20
PCAT-8	535.39 ± 3.58	9.06 ± 0.33	406.07 ± 32.89	44.67 ± 1.76	10.54 ± 0.23	5.02 ± 0.16
PCAT-10	525.94 ± 1.71	9.72 ± 0.37	415.88 ± 46.60	41.94 ± 1.75	8.52 ± 0.48	4.73 ± 0.24

addition of nano-$CaCO_3$ gradually increased the distance between the continuous phases of the material and weakened the interaction between macromolecular chains, which was the main reason for the decrease in the tensile strength of the composite. When the addition ratio of TA content exceeded 2 wt%, the interaction enhanced were formed by $PCaCO_3$@TA combining with the ester group and hydroxyl group of PBSeT, resulting in the recovery of the tensile strength of PACT. However, the modulus of PCAT was improved regardless of the cross-linking point whether $PcaCO_3$@TA or the hydrogen bond formed; the Young's modulus was dropped off due to nano-$CaCO_3$ agglomeration when the content of TA was greater than 4 wt%, which was consistent with the previous analysis.

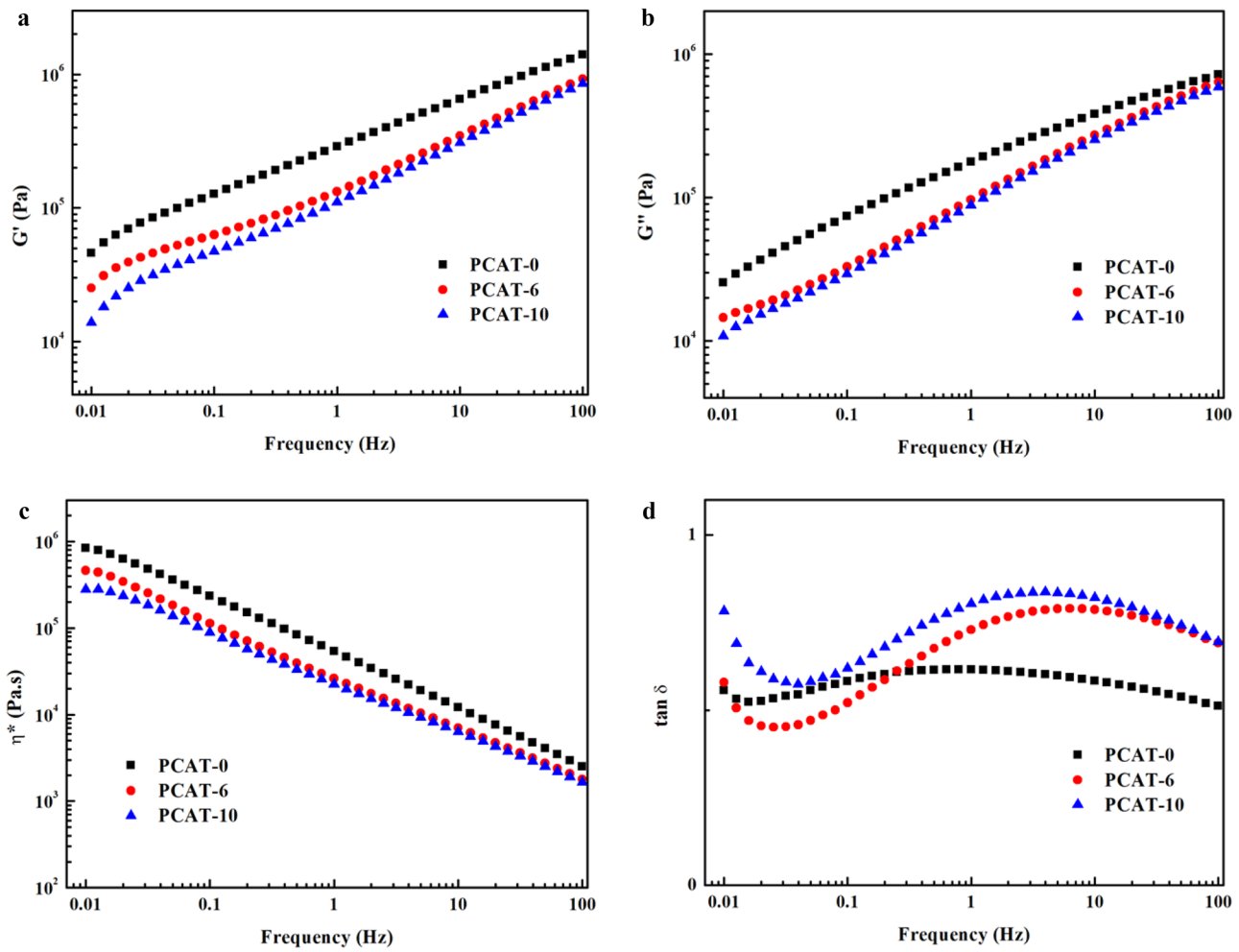

Fig. 7 Rheological behavior of PCAT - (0, 6, and 10) at $T = 140$ °C: **a** storage modulus, G'; **b** loss modulus, G''; **c** complex viscosity, η*; and **d** loss factor (tan δ)

3.6 Rheological measurements

Rheological properties of PCAT composites were analyzed to assure the dispersion state of nano-$CaCO_3$ particles of composite with different content of TA. Figure 7 exhibits the dependence of storage modulus (G'), loss modulus (G"), complex viscosity (η*), and loss factor (tan δ) on frequency for diverse PCAT specimens (sample) at 130 ℃. At low frequency, G' is proportional to ω^2. The slope of the frequency sweep curve in the low frequency region is 2 for pure PBSeT, which is consistent with the rheological behavior of linear polymers in the linear viscoelastic region [36–38]. As shown in Fig. 7a, the slope for of 20 wt% nano-$CaCO_3$ content became smaller, and the aggregation of nanoparticles emerged. With the addition of TA and the formation of $PCaCO_3$@TA, the interaction force between complex and PBSeT got enhanced, and the dispersion of nano-$CaCO_3$ was improved, which was consistent with the corresponding elemental maps of PCAT in Fig. 1. Nevertheless, owing to the hydroxyl groups on the TA surface prompting the aggregation of nano-$CaCO_3$, the mechanical properties of the composites including 10 wt% TA were degraded.

Figure 7c showed that the complex viscosity of PCAT-6 was higher than that of PCAT-10, and the difference in viscosity was only evident at low frequencies. The viscosity of the complex was significantly increased by agglomeration, filler interactions, and surface treatment at lower frequencies, whereas at higher frequencies, the variations in the filler content as well as the nature of the polymer matrix regulate the rheological parameters [39–41]. The decrease of complex viscosity for PCAT-10 was derived from the decrease in the interaction between calcium carbonate and PBSeT caused by $PCaCO_3$@TA formed from the encapsulation of TA on the surface of nano-$CaCO_3$.

Tan δ, equal to loss modulus (G")/G', is a significant analysis criterion in reflecting the viscoelastic performance of polymers [42, 43]. In the light of viscoelastic polymer theory, polymer displayed a liquid-like performance when G" was higher than G'. On the contrary, it exhibited a solid-like behavior [42, 44]. Clearly, the dispersion state was only changed by the formation of $PCaCO_3$@TA, and the final state was determined by the ratio of filler to matrix.

3.7 Enzymatic degradation

The study of the enzymatic degradation behaviors, water absorption rate, and water contact angle of the composites was indispensable to develop novel bio-based biodegradable products. The weight loss of PCAT during enzymatic degradation by lipase in phosphate buffer solution (pH = 7.2) at 25 ℃, water absorption rate, and water contact angle are showed at Fig. 8 and Table 5.

Obviously, the weight loss of the composites was greatly reduced by the addition of nano-$CaCO_3$. Nevertheless, the degradation performance of PCAT with the addition of TA was transformed better than before. The trend, first increased and then decreased, was basically the same for water absorption and the effect of TA on PCAT. In addition, the trend for

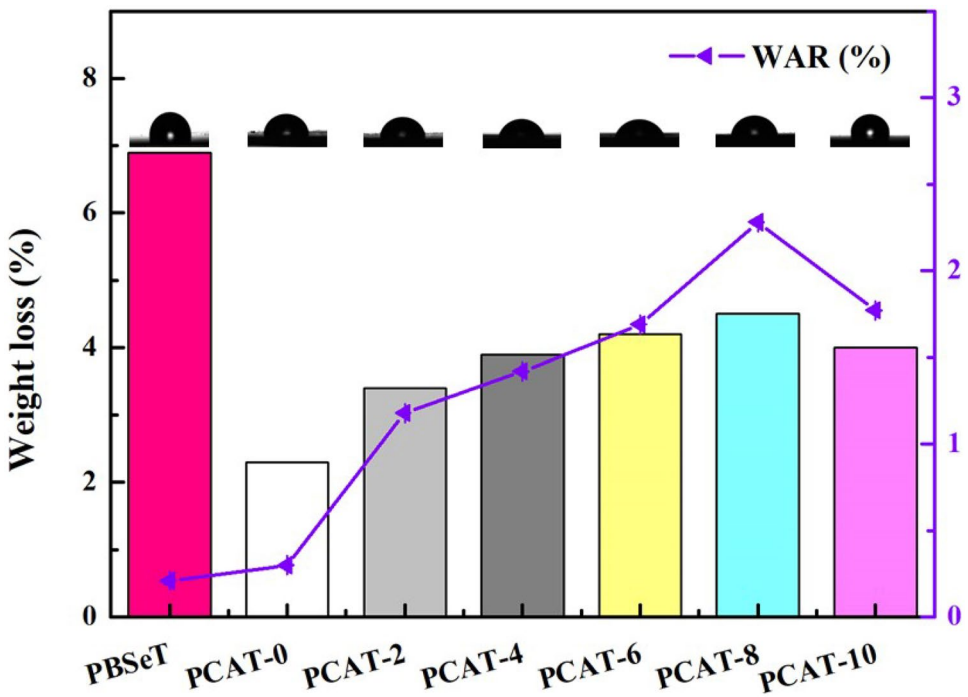

Fig. 8 Weight loss (%) of enzymatic degradation, water absorption rate (%), and water contact angle for composites with different proportions of tannic acid addition

Table 5 Comparison of density, water contact angle, water absorption rate, and weight loss of enzymatic degradation for PCAT composites

Sample	Density (g/cm^3)	Water contact angle (°)	Water absorption rate (%)	Weight loss (%)
PBSeT	1.10 ± 0.023	84.87 ± 1.36	0.21	6.9
PCAT-0	1.26 ± 0.016	77.50 ± 1.42	0.30	2.3
PCAT-2	1.26 ± 0.038	73.06 ± 1.28	1.18	3.4
PCAT-4	1.28 ± 0.030	70.59 ± 0.97	1.42	3.9
PCAT-6	1.30 ± 0.039	65.05 ± 1.45	1.69	4.2
PCAT-8	1.29 ± 0.025	79.19 ± 1.79	2.28	4.5
PCAT-10	1.25 ± 0.046	99.98 ± 1.61	1.77	4.0

the change of water contact angle was consistent with the results of water absorption rate. It is known that the result of enzyme degradation is closely related to the concentration of the substrate. The substrate per unit contact area was decreased, due to the addition of nano-$CaCO_3$, which was an important reason for the degradation. Oppositely, both the water absorption performance and the attachment of enzymes improved with the addition of TA which improve the degradation performance as well. On account of the agglomeration of nano-$CaCO_3$, the degradation performance was initially turned into to decline again when TA was greater than 8 wt%.

Figure 9 showed the SEM of the surfaces of the PCAT composite before and after enzymatic degradation. Originally, the surfaces of PCAT-0, 2, 4, and 6 were smooth. However, when the content of TA exceeded 8 wt%, the composite material had different degrees of surface protrusion caused by the agglomeration of nano-$CaCO_3$. This was consistent with the above analysis results. After enzymatic degradation, the surface became rough and the holes appearing on the surface of PACT with varying content of TA were also different. With the addition of TA, the pores were changed from large to small. It seemed that the enzymatic degradation began from the surfaces of polymer. Moreover, it was noteworthy that the surface of the composite seemingly did not seem be changed when the TA content was attained to 10 wt%, which meant that the degradation might be occurred at the inside of composite material.

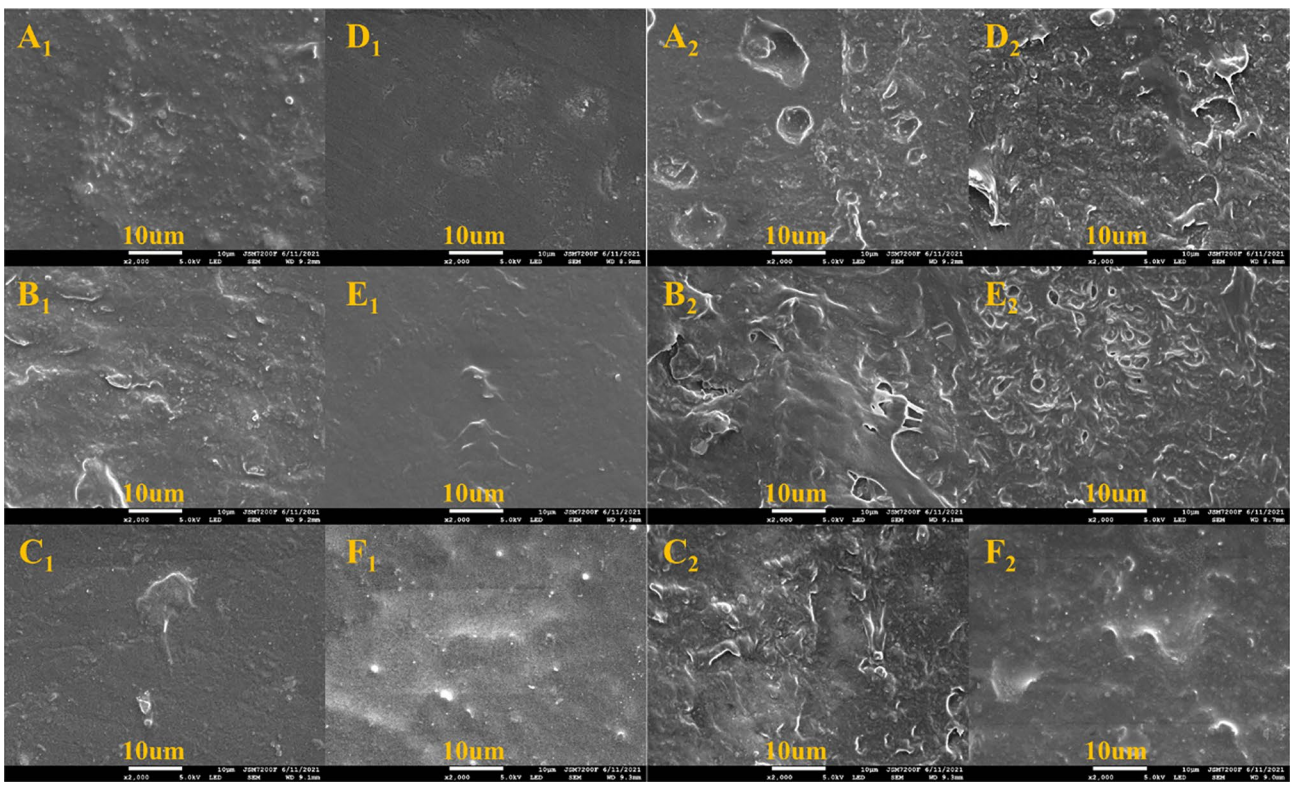

Fig. 9 SEM photographs of composites with different proportions of tannic acid addition before (0 day) and after (36 days) enzymatic degradation. (A_1 and A_2) PCAT-0; (B_1 and B_2) PCAT-2; (C_1 and C_2) PCAT-4; (D_1 and D_2) PCAT-6; (E_1 and E_2) PCAT-8; (F_1 and F_2) PCAT-10

In short, the improvement of thermal stability, puncture performance, and Young's modulus of PACT composite materials will promote its application as a degradable material.

4 Conclusions

PCAT composites were successfully prepared by melt blending method. The glass transition temperature, thermal stability, puncture load, and degradation performance can be improved by changing the ratio of TA. Experimental results showed that the thermal stability, glass transition temperature, and puncture load of composite materials were improved by $PCaCO_3$@TA. When the content of TA was 2, 4, and 6 wt%, the maximum thermal decomposition temperature, Young's modulus, and glass transition temperature of the composite material were advanced by 12.67 ℃, 64.5%, and 10.36 ℃, respectively. Peculiarly, the puncture load of the composite was increased by 71.7% as the TA was 8 wt%, and the degradation performance and water absorption performance were also better than other composites. By means of comprehensive analysis, $PCaCO_3$@TA formed from TA and nano-$CaCO_3$ was mainly aimed at the BSe segment of PBSeT material. In a word, composites derived in this experiment have well application aspect in the field of biodegradable materials.

Supplementary Information The online version contains supplementary material available at https://doi.org/10.1007/s42114-022-00564-6.

Acknowledgements The authors thank Maoyong He of the Taiyuan Institute of Technology for his help.

Author contribution Tong Liu wrote the main manuscript text; Zhimao Li, Tianxiang Jiang, and Shaohua Xi prepared Figs. 1–3; Mina Huang, Hassan Algadi, and Xinming Ye prepared Figs. 4–9 and S1. All authors reviewed the manuscript.

Funding This work is also supported by the Natural Science Basic Research Program of Shaanxi (Grant No. 2022JQ-441).

Declarations

Conflict of interest The authors declare no competing interests.

References

1. Cao Y, Weng M, Mahmoud MHH et al (2022) Flame-retardant and leakage-proof phase change composites based on MXene/polyimide aerogels toward solar thermal energy harvesting. Adv Compos Hybrid Mater 5:1253–1267. https://doi.org/10.1007/s42114-022-00504-4
2. Li H, Huang W, Qiu B et al (2022) Effective removal of proteins and polysaccharides from biotreated wastewater by polyaniline composites. Adv Compos Hybrid Mater 5:1888–1898. https://doi.org/10.1007/s42114-022-00508-0
3. Jing X, Li Y, Zhu J et al (2022) Improving thermal conductivity of polyethylene/polypropylene by styrene-ethylene-propylene-styrene wrapping hexagonal boron nitride at the phase interface. Adv Compos Hybrid Mater 5:1090–1099. https://doi.org/10.1007/s42114-022-00438-x
4. Tsai P (2020) Performance of masks and discussion of the inactivation of SARS-CoV-2. Eng Sci 10:1-7. https://doi.org/10.30919/es8d1110
5. Shafiur Rahman GM, Aftab H, Shariful Islam M et al (2016) Enhanced physico-mechanical properties of polyester resin film using CaCO3 filler. Fibers Polym 17:59–65. https://doi.org/10.1007/s12221-016-5612-y
6. Yan D, Wang Z, Guo Z et al (2020) Study on the properties of PLA/PBAT composite modified by nanohydroxyapatite. J Mater Res Technol 9:11895–11904. https://doi.org/10.1016/j.jmrt.2020.08.062
7. Pan D, Su F, Liu H et al. (2021) Research progress on catalytic pyrolysis and reuse of waste plastics and petroleum sludge. ES Mater Manufac 11:3-15. https://doi.org/10.30919/esmm5f415
8. Tian J, Fan R, Zhang Z et al (2022) Flexible and biocompatible poly (vinyl alcohol)/multi-walled carbon nanotubes hydrogels with epsilon-near-zero properties. J Mater Sci Technol 131:91–99. https://doi.org/10.1016/j.jmst.2022.05.019
9. Sun K, Duan W, Lei Y et al (2022) Flexible multi-walled carbon nanotubes/polyvinylidene fluoride membranous composites with weakly negative permittivity and low frequency dispersion. Compos Part Appl Sci Manuf 156:106854. https://doi.org/10.1016/j.compositesa.2022.106854
10. Cai J, Murugadoss V, Jiang J, et al. (2022) Waterborne polyurethane and its nanocomposites: a mini-review for anti-corrosion coating, flame retardancy, and biomedical applications. Adv Compos Hybrid Mater 5:641–650. https://doi.org/10.1007/s42114-022-00473-8
11. Feng J, Zhang W, Wang L, He C (2020) Performance comparison of four kinds of straw/PLA/PBAT wood plastic composites. BioResources 15:2596–2604
12. Yang F, Qiu Z (2011) Miscibility and crystallization behavior of biodegradable poly(butylene succinate)/tannic acid blends. Ind Eng Chem Res 50:11970–11974. https://doi.org/10.1021/ie201480e
13. Giri J, Lach R, Grellmann W et al (2019) Compostable composites of wheat stalk micro- and nanocrystalline cellulose and poly(butylene adipate-co-terephthalate): surface properties and degradation behavior. J Appl Polym Sci 136:48149. https://doi.org/10.1002/app.48149
14. Hernandez-Lopez M, Nacary Correa-Pacheco Z, Bautista-Banos S et al (2019) Bio-based composite fibers from pine essential oil and PLA/PBAT polymer blend. Morphological, physicochemical, thermal and mechanical characterization. Mater Chem Phys 234:345–353. https://doi.org/10.1016/j.matchemphys.2019.01.034
15. Kim SJ, Kwak HW, Kwon S et al (2020) Synthesis, characterization and properties of biodegradable poly(butylene sebacate-co-terephthalate). Polymers 12:2389. https://doi.org/10.3390/polym12102389
16. Amrita A, Manoj A, Ch R, et al (2022) Biodegradable Filament for 3D Printing Process: A Review. Eng Sci 18:11–19. https://doi.org/10.30919/es8d616
17. Sun K, Dong J, Wang Z et al (2019) Tunable negative permittivity in flexible graphene/PDMS metacomposites. J Phys Chem C 123:23635–23642. https://doi.org/10.1021/acs.jpcc.9b06753
18. Heidarzadeh N, Rafizadeh M, Taromi FA et al (2017) Biodegradability and biocompatibility of copoly(butylene sebacate-co-terephthalate)s. Polym Degrad Stab 135:18–30. https://doi.org/10.1016/j.polymdegradstab.2016.11.013
19. Kim SJ, Kwak HW, Kwon S et al (2021) Characterization of PLA/PBSeT blends prepared with various hexamethylene diisocyanate contents. Materials 14:197. https://doi.org/10.3390/ma14010197

20. Liu T, Lian X, Li L et al (2020) Facile fabrication of fully biodegradable and biorenewable poly (lactic acid)/poly (butylene adipate-co-terephthalate) in-situ nanofibrillar composites with high strength, good toughness and excellent heat resistance. Polym Degrad Stab 171:109044. https://doi.org/10.1016/j.polymdegradstab.2019.109044
21. Chang B, Li Y, Wang W et al (2021) Impacts of chain extenders on thermal property, degradation, and rheological performance of poly(butylene adipate-co-terephthalate). J Mater Res 36:3134–3144. https://doi.org/10.1557/s43578-021-00308-0
22. Rocha DB, Souza de Carvalho J, de Oliveira SA, dos Santos RD (2018) A new approach for flexible PBAT/PLA/CaCO3 films into agriculture. J Appl Polym Sci 135:46660. https://doi.org/10.1002/app.46660
23. Wang X-W, Wang G-X, Huang D et al (2019) Degradability comparison of poly(butylene adipate terephthalate) and its composites filled with starch and calcium carbonate in different aquatic environments. J Appl Polym Sci 136:46916. https://doi.org/10.1002/app.46916
24. Shi X, Zhang G, Liu Y et al (2016) Microcellular foaming of polylactide and poly(butylene adipate-co-terephthalate) blends and their CaCO3 reinforced nanocomposites using supercritical carbon dioxide. Polym Adv Technol 27:550–560. https://doi.org/10.1002/pat.3768
25. Brzeziński M, Socka M, Makowski T et al (2021) Microfluidic-assisted nanoprecipitation of biodegradable nanoparticles composed of PTMC/PCL (co)polymers, tannic acid and doxorubicin for cancer treatment. Colloids Surf B Biointerf 201:111598. https://doi.org/10.1016/j.colsurfb.2021.111598
26. Liang Y, Yang F, Qiu Z (2012) Miscibility and crystallization behavior of biodegradable poly(ε-caprolactone)/tannic acid blends. J Appl Polym Sci 124:4409–4415. https://doi.org/10.1002/app.35430
27. Song P, Jiang S, Ren Y et al (2016) Synthesis and characterization of tannin grafted polycaprolactone. J Colloid Interface Sci 479:160–164. https://doi.org/10.1016/j.jcis.2016.06.056
28. Li Z, Li Y, He M et al (2022) Effects of the species of crosslinking reagents on the structures and properties of biodegradable poly (butanediol sebacate - butanediol terephthalate) copolyester. J Appl Polym Sci 139:52145. https://doi.org/10.1002/app.52145
29. Li Z, Li Y, Dong X et al (2021) Synthesis, characterization and properties of poly(butanediol sebacate–butanediol terephthalate) (PBSeT) copolyesters using glycerol as cross-linking agent. Mater Today Commun 28:102557. https://doi.org/10.1016/j.mtcomm.2021.102557
30. Li Z, Li Y, Lei H et al (2022) The effect of synergistic/inhibitory mechanism of terephthalic acid and glycerol on the puncture, tearing, and degradation properties of PBSeT copolyesters. Adv Compos Hybrid Mater 5:1335–1349. https://doi.org/10.1007/s42114-021-00405-y
31. Zhang CY, Lu H, Zhuang Z et al (2010) Nano-hydroxyapatite/poly(l-lactic acid) composite synthesized by a modified in situ precipitation: preparation and properties. J Mater Sci Mater Med 21:3077–3083. https://doi.org/10.1007/s10856-010-4161-y
32. Xiao D, Cheng J, Liang W et al (2021) Metal-phenolic coated and prochloraz-loaded calcium carbonate carriers with pH responsiveness for environmentally-safe fungicide delivery. Chem Eng J 418:129274. https://doi.org/10.1016/j.cej.2021.129274
33. Zhang T, Yu Q, Fang L et al (2019) All-organic multilayer coatings for advanced poly(lactic acid) films with high oxygen barrier and excellent antifogging properties. ACS Appl Polym Mater 1:3470–3476. https://doi.org/10.1021/acsapm.9b01030
34. Li X, Tan D, Xie L et al (2018) Effect of surface property of halloysite on the crystallization behavior of PBAT. Appl Clay Sci 157:218–226. https://doi.org/10.1016/j.clay.2018.02.005
35. Mukherjee T, Czaka M, Kao N et al (2014) Dispersion study of nanofibrillated cellulose based poly(butylene adipate-co-terephthalate) composites. Carbohydr Polym 102:537–542. https://doi.org/10.1016/j.carbpol.2013.11.047
36. Ying Z, Wu D, Wang Z et al (2018) Rheological and mechanical properties of polylactide nanocomposites reinforced with the cellulose nanofibers with various surface treatments. Cellulose 25:3955–3971. https://doi.org/10.1007/s10570-018-1862-8
37. Wang Y, Weng F, Li J et al (2018) Influence of phase separation on performance of graft acrylic pressure-sensitive adhesives with various copolyester side chains. ACS Omega 3:6945–6954. https://doi.org/10.1021/acsomega.8b00737
38. Zuber M, Corda J. Souza A et al (2022) Formaldehyde concentration in an anatomical dissection room with three different ventilation configurations using computational fluid dynamics. Eng Sci 18:177–186. https://doi.org/10.30919/es8d674
39. Zhang T, Zhang C, Yang Y et al (2021) Improved properties of poly(butylene adipate-co-terephthalate)/calcium carbonate films through silane modification. J Appl Polym Sci 138:50970. https://doi.org/10.1002/app.50970
40. He M, Gu K, Wang Y et al (2021) Development of high-performance thermoplastic composites based on polyurethane and ground tire rubber by in-situ synthesis. Resour Conserv Recycl 173:105713. https://doi.org/10.1016/j.resconrec.2021.105713
41. Arun A, Malrautu P, Laha A, Ramaksihna S et al (2021) Gelatin nanofibers in drug delivery systems and tissue engineering. Eng Sci 16:71–81. https://doi.org/10.30919/es8d527
42. Li Y, Yin D, Liu W et al (2020) Fabrication of biodegradable poly (lactic acid)/carbon nanotube nanocomposite foams: significant improvement on rheological property and foamability. Int J Biol Macromol 163:1175–1186. https://doi.org/10.1016/j.ijbiomac.2020.07.094
43. Maddadi B, A L, Devesh S, Rao A. Shenoy G, Wijerathne H, Sooriyaperkasam N, Kumar Prasanna et al (2022) Repurposing plastic wastes in non-conventional engineered wood building bricks for constructional application – a mechanical characterization using experimental and statistical analysis. Eng Sci 18:329–336. https://doi.org/10.30919/es8d696
44. Hu X, Lu Y, Li M et al (2018) Effect of montmorillonite on the crystallization, rheological and physical behavior of polyamide-6/polylactic acid blends. Polym Sci Ser A 60:229–238. https://doi.org/10.1134/S0965545X18020062